ELSEVIER

Journal of Chromatography A, 772 (1997) 369–384

JOURNAL OF CHROMATOGRAPHY A

Electrophoretic behaviour of fully sulfonated polystyrenes in capillaries filled with entangled polymer solutions

Hervé Cottet, Pierre Gareil*

Laboratoire d'Electrochimie et de Chimie Analytique, (URA CNRS 216), Ecole Nationale Supérieure de Chimie de Paris, 11 Rue Pierre et Marie Curie, 75231 Paris Cedex 05, France

Abstract

Very little work has been reported so far on the separation of synthetic or industrial polyelectrolytes by CE. Following the pioneering work by Poli and Schure (Anal. Chem., 64 (1992) 896), a more extensive study was undertaken on the separation of standard sodium polystyrenesulfonates (PSS), with molecular masses ranging between 16 and 990×10^3, in capillaries filled with entangled hydroxyethylcellulose (HEC, M_r 250×10^3) or polyethyleneoxide (PEO, M_r 100×10^3) solutions as sieving media. Both bare and polyethyleneglycol (PEG) coated silica capillaries were successfully carried out for achieving the separation. As a consequence, the detection order was easily inverted. Nevertheless, PEG-coated capillaries should not be used in conjunction with chemically similar PEO solutions, owing to PSS–PEG interactions. In order to analyze the electrophoretic behaviour of PSS in these polymer solutions, viscosity measurements directly performed using the CE instrument enabled us to estimate some characteristic polymer parameters such as the radii of gyration, monomer dimensions, entanglement thresholds as well as average pore sizes of the separating network. The influence of the nature and concentration of the separating polymer, the nature of the buffer counter-ion, the ionic strength and the field strength are presented in detail. The PSS migration regimes are also analyzed on the basis of classical models (Ogston, modified Ogston, reptation, biased reptation) that were initially established to account for DNA migration in permanent gels. The impact of PSS molecular masses and conformation and of network pore size is highlighted.

Keywords: Entangled polymers; Capillary columns; Polystyrenesulfonates; Polyelectrolytes

1. Introduction

Synthetic ionic polymers find use in an array of industrial applications, e.g. as thickeners, dispersing or flocculating agents [1]. The characterization of their average molecular mass and charge and of their related distributions, the elucidation of their structure and the knowledge of their overall physico-chemical properties is becoming increasingly important for the improvement of their performances and the development of their applications. The techniques of choice that are carried out with this prospect to date are microanalysis, NMR, size-exclusion chromatography combined with refractive index detection, viscosimetric or light scattering measurements and gas chromatography coupled on the inlet side to pyrolysis and on the outlet side to mass spectrometry. Direct electrospray ionization mass spectrometry is also gaining acceptance as it can provide accurate determination of their molecular mass.

Capillary electrophoresis, on which there has been focused a great deal of attention for the separation and characterization of biological macromolecules in the last decade [2], presents a great advantage over conventional chromatographic techniques by operating in a single aqueous phase system, thus preclud-

*Corresponding author.

0021-9673/97/$17.00
PII S0021-9673(96)01057-6

ing any unwanted interaction with a solid phase. It should also allow one to investigate the behaviour of ionic polymers under mild assay conditions which are closer to their industrial applications. These specific assets, besides others commonly recognized such as speed and high resolving power, has prompted pioneering works on poly(oxyalkylene)- and poly(alkyloxide) diamines [3,4], polystyrenesulfonates [5,6], polyaminoacids [7,8] and charged polysaccharides [9,10]. It is now well established that electrophoretic separations of ionic polymers in free solutions is restricted to early oligomers or to analytes differing in their charge to molecular mass ratios. For linear polymers having such an identical ratio, a separating network is required to induce a stronger dependence of analyte friction coefficient on molecular mass, and, thus, allow separation according to the degree of polymerization [11]. The great deal of work that has been accomplished on proteins and especially nucleic acid fragments has resulted in improved understanding of migration mechanisms in these networks and in the elaboration of theoretical migration models (Ogston [12], modified Ogston [13,14], biased reptation models [15,16]). In classical electrophoresis the separating networks consisted of chemical gels such as crosslinked polyacrylamide or a physical gel such as agarose. The emergence of CE has resulted in the introduction of new networks, especially those made up by semi-dilute, entangled hydrophillic polymer solutions, which more easily allow one to avoid air bubble formation inside the capillaries and they can be renewed before each run. To the best of our knowledge, the above migration models have never been applied to macromolecule families other than nucleic acids and proteins.

The purpose of this work was to more deeply investigate the separation of standard polystyrenesulfonates (PSS) with molecular masses ranking between 16 and 990×10^3 in capillaries filled with entangled solutions of hydroxyethylcellulose and polyethyleneoxide and to study if the previously described models account for the migration of the synthetic polymers in these media. In order to better analyze the electrophoretic data, preliminary viscosity measurements were performed, directly using the CE instrument, to allow estimation of the main characteristic polymer parameters such as the radii of gyration, the monomer dimensions, the entanglement thresholds as well as the average pore sizes of the separating network. The impact on the separation of the electric field, the nature and concentration of the separating polymer, the ionic strength and the nature of the buffer counter-ion were also considered.

2. Theoretical background

The following paragraphs are just intended to recall the way the main polymer characteristics can be estimated and the basic relationships for electrophoretic mobility that have been evaluated.

2.1. Polymer characteristics

2.1.1. Entanglement threshold

The entanglement threshold of a polymer corresponds to the concentration C^* above which polymer chains begin to overlap, also referred to as the transition between dilute and semi-dilute solutions. From the theory developed by Grossman and Colburn [11], C^* can be expressed in unit of mass concentration as:

$$C^* = \frac{\frac{3}{4\pi}M_w}{R_g^3 N_A} = \frac{\frac{3}{4\pi}NM_0}{R_g^3 N_A} \quad (1)$$

where M_w is the weight-average molecular mass, N is the number of monomers per polymer chain, M_0 is the monomer molecular mass, R_g is the radius of gyration and N_A is the Avogadro number. Moreover, in an athermal solvent [11]:

$$R_g = aN^{0.6} \quad (2)$$

where a is the monomer dimension. Substituting for R_g in Eq. (1) leads to:

$$C^* = \frac{\frac{3}{4\pi}N^{-0.8}M_0}{N_A a^3} \quad (3)$$

This relationship shows that the entanglement threshold decreases when the polymer molecular size, N, increases. In this work, experimental access to the entanglement threshold was obtained from the viscosity measurements, as suggested by Mitnik et al. [17], by the relationship:

$$C^* = \frac{1.5}{[\eta]} \quad (4)$$

in which the intrinsic viscosity $[\eta]$ can be experimentally determined as an extrapolation of the reduced viscosity, $\eta_{red} = (\eta - \eta_0)/\eta_0 C$, when the polymer concentration, C, goes down to zero. η is the measured polymer solution viscosity and η_0 is the solvent or plain buffer viscosity.

2.1.2. Radius of gyration

If the intrinsic viscosity and the weight-average molecular mass of a polymer are known, the radius of gyration R_g can be estimated using the relationship [11,18]:

$$R_g = \left(\frac{[\eta]M_w}{K6^{3/2}}\right)^{1/3} \quad (5)$$

where K is a universal constant equal to 2.1×10^{23}. The monomer dimension, a, was then determined using Eq. (2).

2.1.3. Screening length and blob size

Beyond the entanglement threshold, the screening length ξ can be defined from the theory of semi-dilute solutions [17,19], corresponding to the distance above which the excluded volume interactions are screened by other chains:

$$\xi(C) = 0.5R_g\left(\frac{C}{C^*}\right)^{-0.75} \quad C > C^* \quad (6)$$

$\xi(C)$ also corresponds to the average distance between polymer chains. Mitnik et al. [17] preferred introducing the 'blob' size ξ_b, related to ξ by a universal factor:

$$\xi_b = 2.86\xi = 1.43R_g\left(\frac{C}{C^*}\right)^{-0.75} \quad C > C^* \quad (7)$$

The polymer chain can be viewed as a random walk of independent subunits of size ξ_b. It is possible to get an estimation of ξ_b from the calculations of R_g and C^* derived from viscosity measurements. Inserting Eqs. (2,3) into Eq. (7) yields:

$$\xi_b(C) = 1.43\frac{M_0^{0.75}N_A^{-0.75}}{a^{1.25}}C^{-0.75} \quad C > C^* \quad (8)$$

The blob size, which can be regarded as an estimation of the pore size of the network, depends on the polymer concentration and on its nature through the ratio $M_0^{0.75}/a^{1.25}$ but remains independent of polymer chain length N.

2.2. Migration models

2.2.1. Ogston model: Molecular sieving

In the Ogston model [11,12,18], the solute, considered as an undeformable sphere of radius R_g, migrates through a random network of linear polymers. Using geometrical considerations, the mobility μ of a solute in the polymer network can be expressed as:

$$\log \mu = \log \mu_0 - K(r + R_g)^2 C \quad (9)$$

where μ_0 is the free solute mobility (i.e. without the network), C is the sieving polymer concentration or the gel concentration, r is the thickness of the polymer strand and K a constant. $K_r = K(r+R_g)^2$ is called the retardation coefficient.

According to this model the graph of $\log \mu$ versus C, known as the Ferguson plot, should be a straight line with the slope being equal to the retardation coefficient. The linearity of the Ferguson plot is a necessary but not sufficient condition to infer that a solute follows the Ogston regime. In addition to this, the graph giving $\sqrt{K_r}$ versus R_g must be linear. However, this last representation can only be realized if solute R_g is known.

In a recent paper [20], Slater and Guo have challenged the basis of the Ogston model, especially the assumption that the electrophoretic mobility is proportional to the fractional volume of the gel. The new model developed, based on a Monte-Carlo computer simulation, concludes that the Ferguson plot is intrinsically non-linear. However, at this time, there is no simple alternative to the Ogston model capable of describing three-dimensional sieving.

2.2.2. Modified Ogston model: Solute elongation

According to Lukey and Smith [14], it can be assumed that the solute will become distorted, ellipsoidal in shape, under high applied electric fields. The relative elongation $\Delta R/R$ of the solute radius is then given by:

$$\frac{\Delta R}{R} = \frac{(R_g - R'_g)}{R_g} = \frac{\sqrt{K_r} - \sqrt{K'_r}}{R_g p} \quad (10)$$

where R'_g is the stretched solute radius defined as the radius of its circular cross-section, K'_r is the observed retardation coefficient of the solute having a radius of gyration R_g before deformation, K_r is the retardation coefficient extrapolated for low electric fields (i.e., corresponding to a pure Ogston regime) and p is the slope of the linear portion of the graph giving $\sqrt{K'_r}$ versus R_g.

2.2.3. Reptation and biased reptation models

When a linear flexible polymer is forced to migrate through a network having a mesh size smaller than R_g, the polymer chain moves head first by a reptile-like motion and its electrophoretic mobility is a decreasing function of molecular size N. This regime has been called pure reptation. Moreover under a strong electric field, the polymer becomes oriented and stretched. Consequently, the mobility increases as the field strength increases. This latter regime has been called biased reptation. The following relationship between the electrophoretic mobility of a polymer μ, molecular size N and field strength E has been proposed from scaling arguments [15,18]:

$$\mu = K\left(\frac{1}{N} + bE^2\right) \quad (11)$$

where K is a constant, and b is a function of the solute and the network. This relationship shows that the dependence of the mobility on the molecular size is maximal in the pure reptation regime and it decreases for high electric fields and/or very large solutes.

Plotting $\log \mu$ versus $\log N$ has been recognized as a convenient way to identify deviations from pure reptation [17,21].

3. Experimental

3.1. CE instrumentation

All electrophoresis experiments were performed using an Applied Biosystems (ABI) Model 270 A capillary electrophoresis instrument (Santa Clara, CA, USA). The temperature setting was 27°C. Samples were introduced hydrodynamically by the application of a negative pressure of 16.7 kPa on the outlet side of the capillary. Solutes were monitored spectrophotometrically at their local absorbance maximum of 225 nm. Data were recorded on a Spectra-Physics (San Jose, CA, USA) 4400 integrator.

3.2. Chemicals

The polystyrenesulfonate standards (PSSs, M_r 16, 41, 88, 177, 350 and 990×10^3, 80–100% sulfonated), were purchased from American Polymer Standards (Mentor, OH, USA), under their sodium salt form. M_r 250×10^3 hydroxyethylcellulose (HEC), M_r 100×10^3 polyethyleneoxide (PEO) and mesityl oxide were from Aldrich (Milwaukee, WI, USA). Purified water delivered by an Alpha-Q system (Millipore, Molsheim, France) was used to prepare all buffers and standard solutions. Borate buffers (pH 9.2) were prepared with borax (disodium tetraborate, decahydrate) from Prolabo (Paris, France). Separating network solutions were made up by slowly adding HEC (PEO, respectively) powder to the borate buffer, then allowing it to dissolve for several hours at 50–60°C (60–70°C, respectively), and then overnight at room temperature, under gentle mechanical stirring. PEO solutions were additionally allowed to settle for 1 day at room temperature and the supernatant part was clarified using a 0.5 μm pore size filter unit. All solutions were finally degassed using a water aspirator. PSS stock sample solutions were prepared at a concentration of 5 g/l in water and then diluted 10 fold with the borate buffer. Mesityl oxide was used as a 0.1% (v/v) solution in the borate buffer for the determination of the electroosmotic mobility.

3.3. Separation columns

Two types of capillaries were used as separation compartment: (i) 45 cm (25 cm to the detector)×50 μm I.D. bare silica capillaries purchased from Supelco, Bellefonte, PA, USA. (ii) 45 cm (25 cm to the detector)×100 μm I.D. DB-WAX (PEG coated,

0.2 μm film thickness) capillaries purchased from J&W (Folson, CA, USA). New PEG coated capillaries were conditioned with methanol for 20 min, water for 5 min and the separating electrolyte (about two capillary volumes). Between runs, they were flushed with about two capillary volumes of separating electrolyte. New uncoated capillaries were conditioned by performing the following washes: 1 *M* NaOH for 10 min, 5 m*M* NaOH solution containing 0.5 *M* NaCl for 10 min, water for 5 min and the separating electrolyte (three capillary volumes). Between runs they were flushed unless otherwise noted with 0.1 *M* NaOH for 3 min, plain buffer for 1 min and finally flushed with about two capillary volumes of separating electrolyte. The time required for rinsing the capillaries with twice their volume of separating electrolyte is dependent on the electrolyte viscosity and is given in Table 1.

3.4. Viscosity measurements

Viscosity measurements were performed at 27°C for various polymer concentrations, below and above the expected entanglement threshold, directly using the CE apparatus, as suggested in a recent paper [22]. The CE apparatus was equipped with an 85 cm (60 cm to the detector)×100 μm I.D. PEG coated capillary (J&W). HEC and PEO solutions were prepared in a 40 m*M* borate buffer as described above. For each solution, two determinations were obtained according to the following reversed protocols. For the first one, the capillary and the outlet buffer reservoir were initially filled with plain borate buffer while the inlet buffer reservoir contained the polymer solution. This solution was sucked into the capillary applying the partial vacuum line provided by the instrument for filling/rinsing purposes. The specific viscosity of the solution was calculated from the time T_1 taken by the solution to reach the detection window:

$$\eta_{sp} = \frac{\eta - \eta_0}{\eta_0} = \frac{d_c^2}{16l^2}\frac{\Delta P T_1}{\eta_0} - 2\frac{L}{l} \quad (12)$$

L and l are the total capillary length and the length to detection window, respectively, d_c is the capillary inner diameter, ΔP is the pressure differential applied by the instrument (66.8 kPa) and η_0 is the viscosity of the plain borate buffer, assimilated to that of water (0.854 cP). For the second determination, the capillary and the outlet reservoir were filled with the polymer solution and the inlet reservoir was filled with the plain borate buffer. The specific viscosity of the solution was then derived from the time T_2 taken by the plain buffer to reach the detection window:

$$\eta_{sp} = \frac{d_c^2}{16l^2}\frac{\Delta P T_2}{\eta_0}\frac{1}{2L-1} - \frac{2L}{2L-1} \quad (13)$$

The time T_{cap} required for flushing a capillary initially filled with plain borate buffer with twice its volume of a polymer solution of known viscosity η was calculated according to the equation:

Table 1
Hydrodynamic and electroosmotic data for HEC and PEO solutions in 40 m*M* borate buffer, pH 9.2, as a function of their concentration

HEC				PEO			
C (g/100 ml)	η (cP)	T_{cap} (s)	m_{eo} (10^{-5} cm^2 V^{-1} s^{-1})	C (g/100 ml)	η (cP)	T_{cap} (s)	m_{eo} (10^{-5} cm^2 V^{-1} s^{-1})
0.1	1.5	105	–	0.5	1.6	110	49.8
0.3	2.7	175	58.2	1.0	2.1	140	39.8
0.5	4.5	280	50.9	1.5	3.4	215	–
0.7	7.2	440	48.5	2.0	4.8	300	33.5
1.0	13.6	810	–	3.0	7.1	430	25.1
1.5	37.5	2200	46.0	5.0	19.4	1150	–

Temperature: 27°C.

η: polymer solution viscosity; T_{cap}: time required for flushing a 50 μm I.D.×45 cm capillary initially filled with plain borate buffer with twice its volume of polymer solution, calculated from Eq. (13) for a pressure differential of 66.8 kPa. m_{eo}: electroosmotic mobility produced in bare silica capillaries.

$$T_{cap} = \frac{16(\eta_0 + 3\eta)L^2}{d_2^2 \Delta P} \quad (14)$$

3.5. Conductivity measurements

A CDM 3 conductimeter fitted with a measuring cell (CDC 304) of 1 cm^2 surface area (Radiometer, Copenhagen, Denmark) was used for measuring the conductivity of solutions of HEC and PEO in 40 m*M* sodium borate buffer, pH 9.2.

4. Results and discussion

4.1. Viscosity measurements

As a groundwork for this study, viscosity measurements were performed for both polymer analytes (PSS of molecular masses 16, 177 and 990×10^3) and the two separating networks studied (PEO and HEC) in order to confront the respective dimensions of the molecules to separate from those of the separating screens. In this section, the ionic strength has been set up to 40 m*M* which is the value usually investigated afterwards. It was found to be very convenient and straightforward to use the CE instrumentation for this purpose, as already practised by Bello et al. [22]. The viscosity values were thus obtained in exactly the same conditions (electrolyte medium, temperature) as those employed later for CE separation, following the double experimental protocol described above. Table 1 gives the viscosity values for HEC and PEO concentrations of interest and the times required for flushing a capillary with twice its volume of polymer solution, which was considered to be an order of magnitude of the equilibration time. Fig. 1 shows the logarithmic plot of the specific viscosity versus the polymer concentration for PEO and HEC. As expected from the theory of semi-dilute solutions, a linear part of the slope unity was obtained experimentally. The same behaviour was observed for the three PSS studied (graphs not shown). However, as emphasized by Viovy and Duke [16], this graph shows that it would be difficult to determine the entanglement threshold from the deviation of the experimental points from linearity. C^* was preferably calculated from Eq. (4),

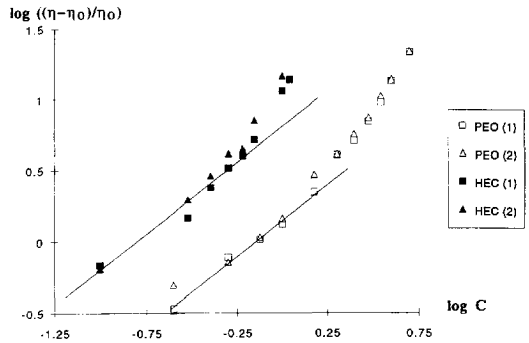

Fig. 1. Variation of the specific viscosity of PEO and HEC solutions as a function of polymer concentration. Experimental protocol, see Section 3. Indices (1) and (2) refer to data points obtained with the capillary initially filled with plain electrolyte and polymer solution, respectively. The straight lines drawn are the ones of slope unity fitting the points corresponding to $C<C^*$.

after extrapolation of the reduced viscosity to a zero concentration of polymer to get the intrinsic viscosity. Nevertheless, the C^* values obtained (0.5 g/100 ml for HEC, 1.8 g/100 ml for PEO) remain consistent with the onset of linearity deviation observed in Fig. 1.

The physico-chemical characteristics derived from the viscosity measurements for both PSS and sieving media are given in Table 2. From the three PSS studied, the following relationship was established by least-square fitting:

$$R_g(\text{nm}) = 0.0048 M_r^{0.69} \quad (15)$$

This relationship was used to derive the values for the radii of gyration of the other PSS standards. For HEC and PEO, the M_r values given by the supplier were checked using the empirical Mark-Houwink relationship and the experimental value of $[\eta]$:

$$[\eta] = K M_r^b \quad (16)$$

and the K and b values for water as solvent are found in the literature: $K=9.53\times10^{-3}$ and $b=0.83$ for HEC [11] and $K=6.4\times10^{-3}$ and $b=0.82$ for PEO [23]. The calculated M_r values were 107×10^3 for PEO and 256×10^3 for HEC, in good agreement with the supplier's values. The uncertainty on the monomer molecular mass of HEC, resulting from the unknown derivatization rate, has led us to give two limiting values for the monomer dimension. From

Table 2
Physicochemical characteristics of the polymers studied derived from viscosity measurements: intrinsic viscosity ([η]), entanglement threshold (C^*), radius of gyration (R_g) and monomer dimension (a)

Polymer (M_r)	[η] (ml/g)	C^* (g/100 ml)	R_g (nm)	a (nm)
PSS (16×10^3)	22.5	6.5	5	0.36
PSS (177×10^3)	125	1.2	19	0.34
PSS (990×10^3)	860	0.2	65	0.40
HEC (250×10^3)	294	0.5	33	0.43(a)/0.54(b)
PEO (100×10^3)	85	1.8	14	0.13

M_r: weight-average molecular mass given by the supplier. [η]: extrapolation of reduced viscosity at zero concentration. C^*: calculated from Eq. (4). R_g: calculated from Eq. (5). a: calculated from Eq. (2), with a monomer molecular mass of 206 for PSS (sodium salt), 44 for PEO and either 187 (a) or 272 (b) for HEC, according to the derivation rate (see Section 4.1).

Eqs. (6,7), it appears that at their respective threshold concentrations, the pore size produced by PEO is more than twice as narrow as that produced by HEC.

The values of the physico-chemical polymer parameters derived from viscosity measurements were next checked for consistency with the theory of semi-dilute solutions. According to Eq. (1), the $C^*R_g^3/M_w$ ratio should be independent of both molecular mass and polymer nature. It can be estimated that the values reported in Table 3 show a very satisfactory agreement with the theory for PEO and for PSS of various molecular masses. A slightly superior value was obtained with HEC, however, which may be due to polymer–polymer or polymer–solvent interactions.

4.2. Conductivity of the sieving polymers

The ionic purity of the neutral hydrophillic polymers used to realize the separating networks is an important issue in view of a study about the influence of the electric field in a wide range. In effect, depending on the applied field and the electrolyte conductivity, the capacity of the thermoregulating device can be exceeded due to Joule heating and any subsequent temperature variation during an experiment will obscure the understanding of the experimental data. The current intensity within the capillary was monitored as a function of applied voltage for the various concentrations of HEC and PEO investigated. A gradual increase in intensity was ascertained on increasing HEC concentration, even in the linear part of the intensity–voltage plot. For PEO solutions, a much less pronounced increase was noticed for concentrations inferior to about the C^* value, and afterwards intensity declined. In order to get rid of heating effects, the conductivity of the HEC and PEO solutions in the 40 mM sodium borate buffer, pH 9.2, used for further separations was then directly measured. Fig. 2 shows the variation of the conductivity of the solutions as a function of the

Table 3
Consistency of the values for physicochemical polymer parameters derived from viscosity measurements (as given in Table 2) with the theory of semi-dilute solutions

Polymer studied (M_w)	$\frac{C^*R_g^3}{M_w}$
PSS (16×10^3)	1.00
PSS (177×10^3)	1.04
PSS (990×10^3)	1.12
PEO (100×10^3)	0.96
HEC (250×10^3)	1.43

See Section 4.1 for comments.

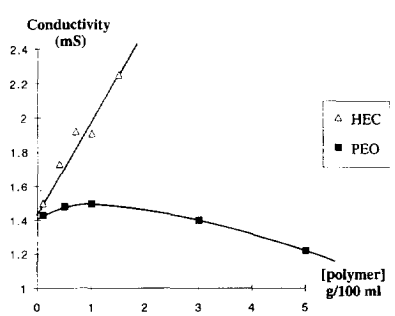

Fig. 2. Variation of the conductivity of HEC and PEO solutions in a 40 mM sodium borate buffer, pH 9.2, as a function of the polymer concentration.

polymer concentration. The common y intercept of both curves corresponds to the expected conductivity of a 40 mM sodium borate buffer, about 0.155 S/m. The conductivity of the HEC solutions increases almost linearly on increasing polymer concentration in the range studied (0–1.5 g/100 ml) whereas for the case of PEO conductivity decreases for concentrations greater than 1 g/100 ml. In the latter case, the conductivity decrease mainly reflects the increase in viscosity of the polymer solution while for the former case the increase in conductivity should be attributed to the presence of ionic impurities in the HEC powder, masking the effect of viscosity. In contrast with PEO, the HEC used contained a significant level of ionic impurities. Assuming the presence of a 1:1 sodium salt and equal molar conductivities for the anion and Na^+ ion, an impurity concentration of 0.5 mM/g HEC can be estimated. As a consequence, the electric field for 50 μm I.D. capillaries should not be in excess of ca. 250 V/cm with HEC and 450 V/cm with PEO to avoid a marked Ohm's law deviation from linearity. Depending on the supplier, the purification of cellulose batches is contemplated for future work.

4.3. Electrophoresis in free solutions

The first electrophoresis experiments were performed in free borate buffer using uncoated and PEG-coated capillaries. A slight alkaline pH buffer was selected throughout this work to ensure high electroosmotic flow in uncoated silica capillaries. As expected, no separation was obtained under these conditions with respect to the analyte molecular mass, as the charge to molecular mass ratio of fully sulfonated polystyrenes remained constant. The electrophoretic mobility values for five PSSs (M_r 16–350×10^3) differ by less than 1.5% from one another. However, the mean values obtained with uncoated and PEG-coated capillaries were 41.2 and 35.4×10^{-5} $cm^2\,V^{-1}\,s^{-1}$, respectively. This significant difference, which could not be explained by the residual contribution of the electroosmotic mobility ($m_{eo}<3\times10^{-5}$ $cm^2\,V^{-1}\,s^{-1}$) suggested the existence of a PSS–PEG interaction, and this was confirmed by the experiment reported in Fig. 3. The build-up of PSSs on the capillary wall resulted in subsequent erratic profiles. The correct initial peak shape could be recovered after flushing the capillary with a surfactant solution. Conversely and contrary to an observation of Poli and Schure [5], no experimental evidence of PSS adsorption on the wall of bare silica capillaries was ascertained.

4.4. Electrophoresis in polymer solutions

As anticipated from the migration models the introduction of a linear polymer such as HEC or PEO in the separation buffer causes PSS electrophoretic mobilities to decrease as molecular mass increases. The PSS separation was investigated in various conditions including the influence of capillary type, polymer nature and concentration, electric field, electrolyte ionic strength and counter-ion.

4.4.1. PEG-coated versus uncoated capillaries

Fig. 4 compares the electropherograms obtained with PEG-coated and uncoated capillaries of equal lengths and under identical electrolyte and sieving conditions. Electroosmotic flow was almost fully suppressed with PEG-coated capillaries so that PSS analytes were injected on the cathodic side and detected on the anodic side in the order of increasing molecular mass. It was also noted that in the presence of entangled HEC in the electrolyte no hint of PSS adsorption on the capillary wall remained apparent. The reverse order of detection can be obtained upon injecting the PSS mixture on the anodic side of an uncoated silica capillary because of the existence of the anodic electroosmotic flow. In effect, although the electroosmotic mobility decreases as HEC or PEO concentration increases (Table 1), it still remains greater than the absolute values of the PSS electrophoretic mobilities. Rinsing procedures between runs have often been recognized to be of key importance for separation repeatability, especially with macromolecules and uncoated silica capillaries. At this point three protocols were tested in detail for separating electrolytes containing 0.5 g/100 ml HEC: (i): no rinsing, renewing of the separating network being only ensured by the electroosmotic flow; (ii): rinsing with the separating electrolyte for 3 min; (iii): successive rinsing with 0.1 M sodium hydroxide and plain borate buffer for 1 min each and with the separating electrolyte for 3 min. A variance analysis performed on the migration

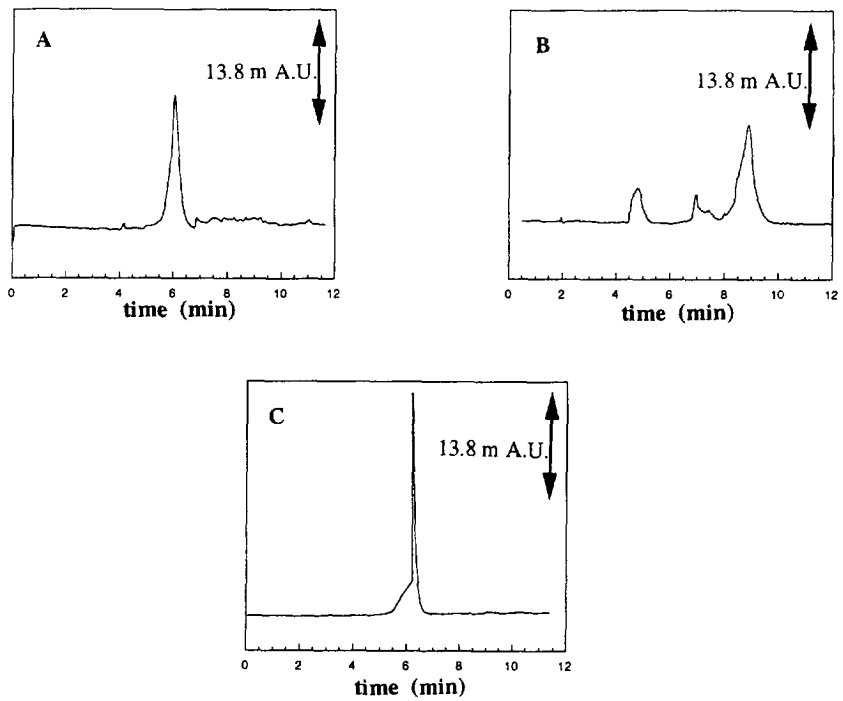

Fig. 3. Experimental evidence of a PSS adsorption on the surface of a PEG-coated capillary. (A) Capillary equilibrated with the electrolyte. (B) Capillary flushed with the PSS sample solution for 10 min, then re-equilibrated with the electrolyte for 10 min. (C) Capillary flushed with 20 m*M* Brij 35 and re-equilibrated with the electrolyte for 10 min. 45 cm (detection, 25 cm)×100 μm I.D. capillary. Electrolyte: 40 m*M* sodium borate buffer, pH 9.2. Applied voltage: −9 kV. Temperature: 27°C. Sample: M_r 88×10^3 PSS, 0.05 g/l. Hydrodynamic injection (1 s, 16.7 kPa).

times (one controlled factor) of the six PSS standards and of mesityl oxide showed that the last protocol gave significantly lower migration time dispersions. This protocol was retained for subsequent work.

4.4.2. Influence of the nature of the separating polymer

The separating performances of HEC and PEO were first compared under identical pore size conditions. Using Eq. (7) and the estimations for R_g and C^* given in Table 2, one obtains:

for HEC (M_r 250 × 10^3):

$$\xi_b(C) = 28.1C^{-0.75} \quad \text{with } C > 0.5 \text{ g/100 ml} \qquad (17)$$

for PEO (M_r 100 × 10^3):

$$\xi_b(C) = 31.1C^{-0.75} \quad \text{with } C > 1.8 \text{ g/100 ml} \qquad (18)$$

where C is expressed in g/100 ml and ξ_b in nm.

The $\xi_b(C)$ relationship obtained for HEC is in excellent agreement with the one ($\xi_b(C) = 27.0C^{-0.72}$) reported by Viovy and Heller [19]. In the case of PEO and HEC solutions similar pore sizes are produced by these polymers at equal concentrations provided that this concentration will simultaneously obey the condition $C > C^*$. Interestingly, it can be ascertained, however, that a 2 g/100 ml PEO solution and a 1.5 g/100 ml HEC solution lead to sieving networks having almost identical ξ_b values (19 nm), though their viscosities are very different (4.8 and 37.5 cP, respectively). Fig. 5A and B exemplify the separations obtained with these sieving networks of identical pore size in a bare silica capillary. In both cases, the baseline resolution of the two largest PSS was not realized (R_s<0.6) because the mesh size of the network is too small compared to the solute dimensions. However, the resolution of the two smaller PSS is better for the HEC solution (R_s=2.2) than for the PEO (R_s=1.2). The global separation of the PSS mixture was better with HEC

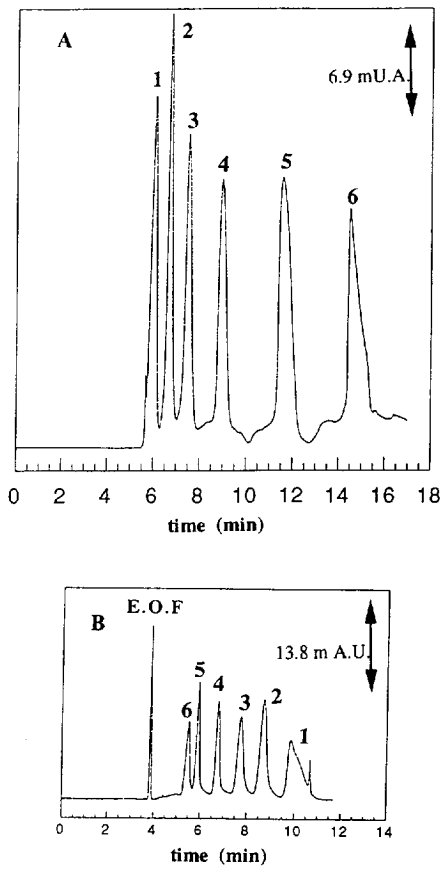

Fig. 4. Separation of a mixture of 6 PSS standards using (A) PEG coated, and (B) uncoated capillaries. Capillary dimensions: 45 cm (detection, 25 cm)×100 μm (A) or 50 μm (B) I.D. Electrolyte: 40 m*M* sodium borate buffer, pH 9.2, 0.7 g/100 ml HEC (η=7.2 cP). Applied voltage: −10 kV (A) or 10 kV (B). Temperature: 27°C. Sample concentration: 0.5 g/l each. PSS molecular mass× 10^3: 16 (1), 41 (2), 88 (3), 177 (4), 350 (5) and 990 (6). Hydrodynamic injection (5 s, 16.7 kPa). UV absorbance at 225 nm. EOF: electroosmotic flow marker.

than with PEO which can be due to the PEO–PSS interaction. The use of a PEO having a higher molecular mass (i.e., closer to the HEC one), should allow us to confront the performances of these polymers for a blob size value more adapted to the solute dimension (e.g., around 50 nm).

From a practical point of view, it is also interesting to compare the analytical performances of the sieving media for a given viscosity, even conclusions cannot be drawn independently of the molecular mass of the polymers. In effect, viscosity becomes an important factor influencing the total analysis time, if rinsing periods between runs are taken into account. In the present study, the PEO concentration required to match the viscosity of a given HEC solution was higher than the HEC concentration because the M_r 100×10^3 PEO chain was shorter than the one of M_r 250×10^3 HEC. Fig. 5B–C on the one hand and Fig. 5D–E on the other hand show pairs of electropherograms that were obtained with HEC and PEO solutions of very similar viscosities. For instance, both polymer solutions presented equal viscosity values, ca. 4.5 cP, at a concentration corresponding to their entanglement threshold C^*. Likewise, slightly above C^*, 7 cP solutions were obtained either by a 3 g/100 ml PEO concentration or a 0.7 g/100 ml HEC concentration, while slightly below C^*, viscosities close to 2.4 cP were produced with 0.3 g/100 ml HEC and 1 g/100 ml PEO solutions (Table 1). To better evaluate the separation mechanisms, blob size values for each of these separating networks were also reported (when defined) in the caption of Fig. 5. These values can be compared with the range of PSS radii of gyration (5–65 nm). For each pair of electropherograms examined, i.e. for a given viscosity, it appears that PEO solutions always yielded poorer resolutions than HEC ones. For example, the resolution of the two heaviest PSSs is inferior to 0.6 in a 4.8 cP PEO solution whereas a 4.5 cP HEC solution yields a resolution of 1.7. This is mainly explained by the fact that a M_r 100×10^3 PEO solution always provides blob sizes that are less adapted to the PSS dimensions than a M_r 250×10^3 HEC solution of the same viscosity. It is also to be noted that the separation was still achieved for sieving polymer concentrations slightly inferior to C^*. Further work is needed in this direction to compare with recent Barron's findings [24,25].

In fact, the ξ_b accessible range for a given separating polymer is limited on its upper side by the entanglement threshold and on its lower side by the highest value of solution viscosity that can be accepted (arbitrary taken here as 20 cP). Fig. 6 shows that the ξ_b ranges that were accessible for M_r 250×10^3 HEC and M_r 100×10^3 PEO were complementary and that the former polymer is much more suitable than the latter for the separation of the mixture of the six PSS standards. The molecular

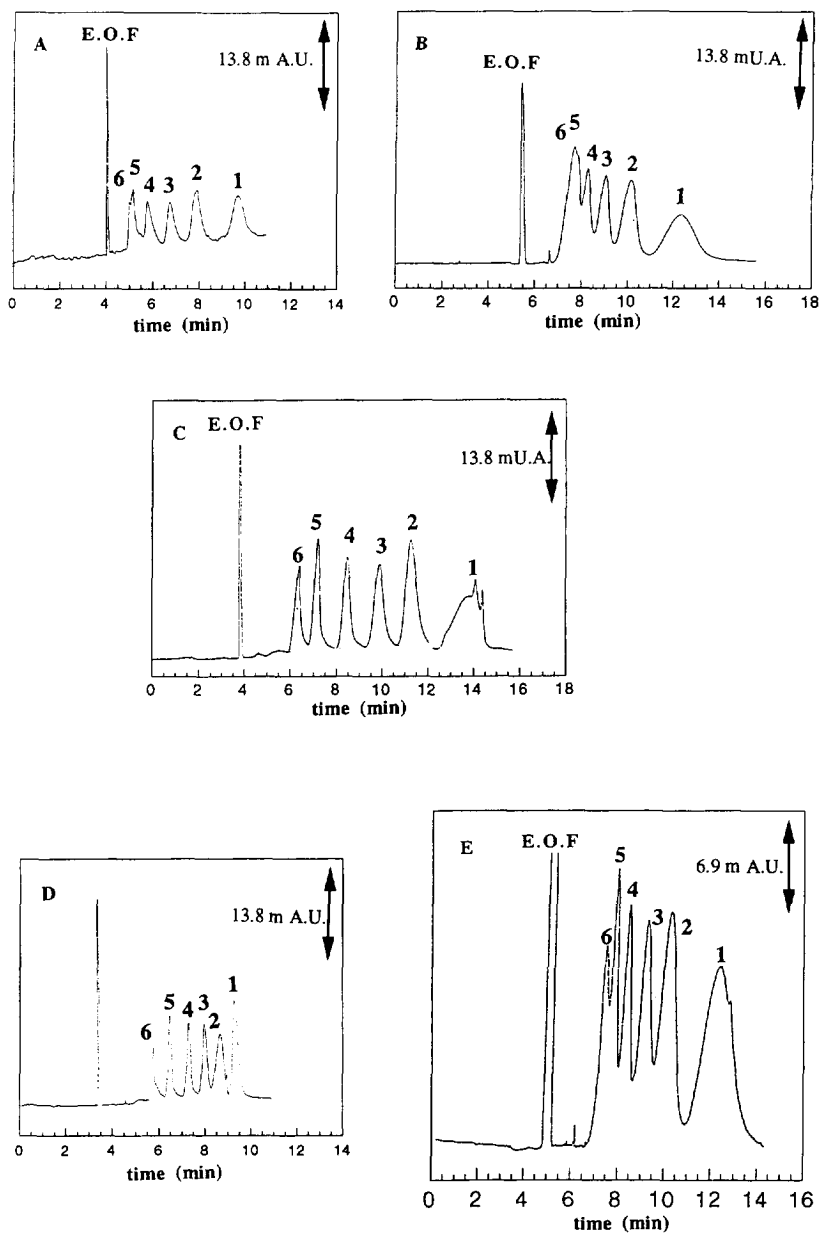

Fig. 5. Impact of the nature and concentration of the separating polymer on the separation of a mixture of six PSS standards. (A) 1.5 g/100 ml HEC, $\xi_b = 20$ nm, $\eta = 37.5$ cP. (B) 2 g/100 ml PEO, $\xi_b = 19$ nm, $\eta = 4.8$ cP. (C) 0.5 g/100 ml HEC, $\xi_b = 47$ nm, $\eta = 4.5$ cP. (D) 0.3 g/100 ml HEC, ξ_b not defined, $\eta = 2.7$ cP. (E) 1 g/100 ml PEO, ξ_b not defined, $\eta = 2.1$ cP. Bare silica capillary: 45 cm (detection, 25 cm)×50 μm I.D. Electrolyte: mentioned polymer solution in 40 m*M* sodium borate buffer, pH 9.2. Applied voltage: 10 kV. Other conditions as in Fig. 4.

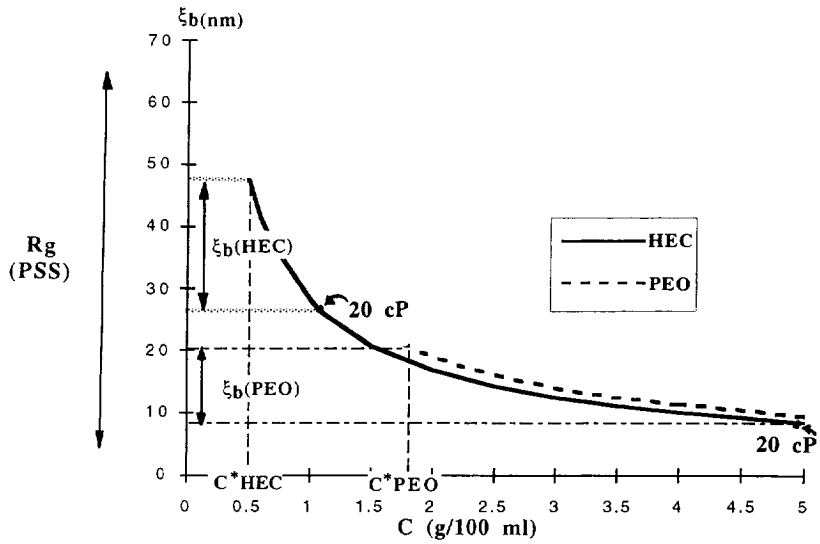

Fig. 6. Comparison of the accessible blob size ranges provided by HEC (M_r 250×10^3) and PEO (100×10^3). See Section 4.4.2 for the definition of these ranges and comments.

mass of the sieving polymer appears to be a key factor for adapting pore size to solute dimension.

4.4.3. Influence of the ionic strength

Ionic strength is usually one of the major parameters influencing the behaviour of polyelectrolytes. Fig. 7 shows that the electrophoretic mobility of the PSS standards decreased (in absolute values) on increasing electrolyte ionic strength. Two effects, working counter to each other, can play a part in this behaviour: (i) an increase in the charge neutralization by sodium counter-ion resulting in a decrease in PSS apparent negative charge, and (ii) a decrease in intramolecular repulsive electrostatic forces, resulting in a decrease in PSS radii of gyration. The results obtained experimentally demonstrate that the prevailing factor was the decrease in the apparent charge. Fig. 8 illustrates the impact of increasing

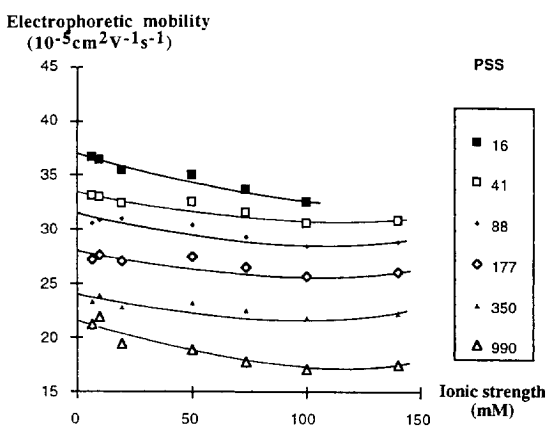

Fig. 7. Influence of electrolyte ionic strength on PSS (molecular mass $\times10^{-3}$ indicated) electrophoretic mobilities. Bare silica capillary: 45 cm (detection, 25 cm)×50 μm I.D. Electrolyte: sodium borate buffers of variable concentrations, pH 9.2, 0.5 g/100 ml HEC. Applied voltage: 10 kV. Other conditions as in Fig. 4.

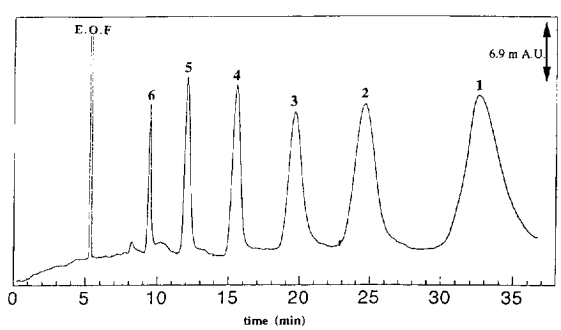

Fig. 8. Impact of increasing electrolyte ionic strength on the separation of a mixture of six PSS standards. Bare silica capillary: 45 cm (detection, 25 cm)×50 μm I.D. Electrolyte: 145 m*M* sodium borate buffer, pH 9.2, 0.5 g/100 ml HEC. Applied voltage: 10 kV. Other conditions as in Fig. 4.

electrolyte ionic strength on the separation of the mixture of six PSS standards. It can be ascertained that the increase in resolution was mainly due to the decrease in electroosmotic mobility, the differences in mobility between neighbour PSS standards remaining almost constant.

4.4.4. Influence of the counter-ion nature

Another important feature influencing both PSS conformation and the apparent charge is the nature of the counter-ion. Fig. 9A shows that on replacing the borate buffer counter-ion in the order: Li^+, Na^+, K^+, Cs^+, the PSS electophoretic mobilities (in absolute values) increased markedly. On the other hand, the electroosmotic mobility decreased, as expected. As in the case of ionic strength, two opposite effects can contribute to the variation of the electrophoretic mobility: (i) a decrease in apparent charge, resulting from increasing affinity of the sulfonate group for the counter-ion in the order $Li^+ < Na^+ < K^+ < Cs^+$, and, consequently (ii) a decrease in radius of gyration. In contrast with what was observed for ionic strength, the latter effect was here the more important.

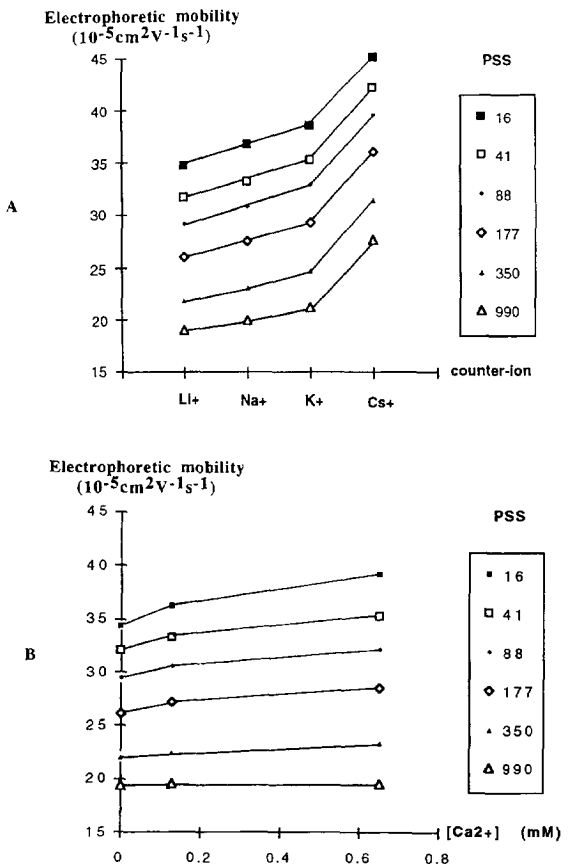

Fig. 9. Influence of the nature of the counter-ion (A, alkali ions; B, calcium ion) on PSS electrophoretic mobility. Bare silica capillary: 45 cm (detection, 25 cm)×50 μm I.D. Electrolyte: (A) 40 m*M* borate buffer with the mentioned cation, pH 9.2, 0.5 g/100 ml HEC. (B) 40 m*M* lithium borate buffer supplemented with the indicated concentration of calcium ion, pH 9.2, 0.5 g/100 ml HEC. Applied voltage: 10 kV. Other conditions as in Fig. 4. PSS as in Fig. 7.

Additional experiments were conducted with lithium borate buffers that were gradually supplemented with small quantities of calcium or barium ions, the overall ionic strength increasing by no more than 5%. The quantity of calcium or barium ions introduced by the electrolyte in the capillary was calculated to be 10–100 times superior to the quantity of sulfonate groups injected. The experimental results obtained exhibited similar electrophoretic behaviours of PSSs in the presence of alkali (Fig. 9A) or alkaline earth (Fig. 9B) ions.

From the point of view of separations, the most favourable selectivity values (defined as the relative differences in mobilities) are obtained with the Li^+ counter-ion. With a bare silica capillary, the best resolutions are obtained with the Cs^+ counter-ion at the expense of the analysis time, because of the slower electroosmotic flow produced. Instead, with PEG-coated capillaries, Li^+-based buffers would lead to the best resolutions and Cs^+-based buffers to the fastest analyze.

4.5. Assessment of migration mechanisms

4.5.1. Ogston regime

As shown in Eq. (9) linear Ferguson plots should be obtained if the Ogston model is obeyed. Strictly, these plots should be drawn with mobilities that were extrapolated to a zero electric field to fully avoid Joule heating and solute stretching and orientation. For the sake of convenience, however, mobility data obtained from experiments performed at an applied voltage of 10 kV (E=220 V/cm) were processed. Fig. 10A shows a Ferguson plot obtained from measurements performed in a bare silica capillary filled with HEC solutions. Except for the two heaviest PSSs, straight lines converging towards a

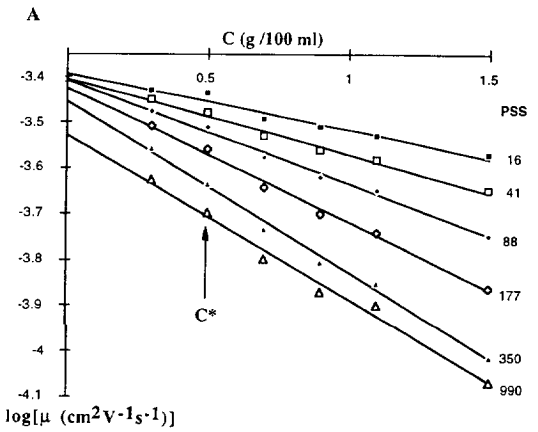

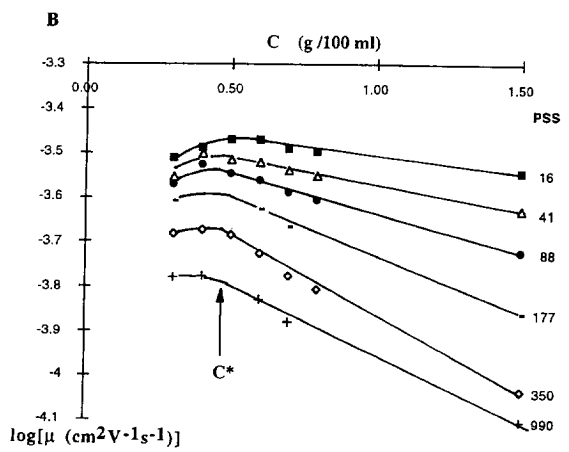

Fig. 10. Ferguson plots in a bare silica (A) and PEG-coated (B) capillaries. Capillary dimensions: 45 cm (detection, 25 cm)×50 μm (A) or 100 μm (B) I.D. Electrolyte: HEC solution in 40 m*M* sodium borate buffer, pH 9.2. Applied voltage: 10 kV. Other conditions as in Fig. 4. PSS as in Fig. 7.

common Y axis intercept are observed, the value of which (39.8×10^{-5} cm^2 V^{-1} s^{-1}) was in very good agreement with the PSS mobility previously determined in the free borate buffer. To better evaluate the domain of validity of the Ogston model, the square root of the retardation coefficient was plotted against the radius of gyration, in accordance with Eq. (9). Fig. 11 clearly shows that the PSSs having a radius of gyration in excess of 15 nm (molecular mass$>120\times10^3$) do not meet the Ogston regime. From the x axis intercept, this graph also allowed us to estimate the thickness of the separating polymer strand, $r=15$ nm. Similar results were obtained in a

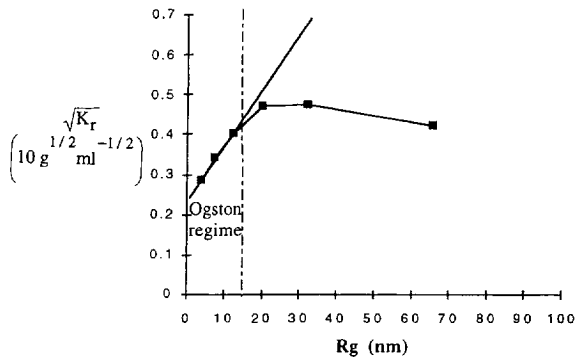

Fig. 11. Domain of validity of Ogston model. Same conditions as in Fig. 10A.

bare silica capillary with PEO solutions, but the upper PSS molecular mass limit for which the Ogston regime is followed was lower than for HEC, in accordance with the narrower pore size produced.

With PEG-coated capillaries, the points corresponding to the lowest HEC concentrations deviated from linearity drastically (Fig. 10B) probably due to the PSS–PEG interaction. For higher HEC concentrations ($C>C^*$), the linear fitting of the experimental plot was observed again, suggesting that entangled HEC prevented the interaction. Lastly, with PEO solutions, erratic electropherograms were obtained whatever the concentration, most likely because PEO does not prevent the interaction between PSS and PEG coating, even for $C>C^*$.

4.5.2. Modified Ogston regime

Table 4 gives the values of the relative elongation $\Delta R/R$ that were estimated from Eq. (10) for the 6 PSSs studied under different electric field strengths. These values can be compared to those reported by

Table 4
Relative elongation $\Delta R/R$ of different PSSs in various electric fields

PSS:M_r	$E=220$ V/cm	$E=445$ V/cm	$E=665$ V/cm
16×10^3	0	0	0
41×10^3	0	0	0
88×10^3	0.08	0.08	0.10
177×10^3	0.23	0.19	0.22
350×10^3	0.39	0.42	0.50
990×10^3	0.71	0.76	0.81

Capillary: bare silica, 50 μm I.D.×45 cm (detection, 25 cm). Electrolyte: HEC solution in a 40 m*M* sodium borate buffer, pH 9.2.

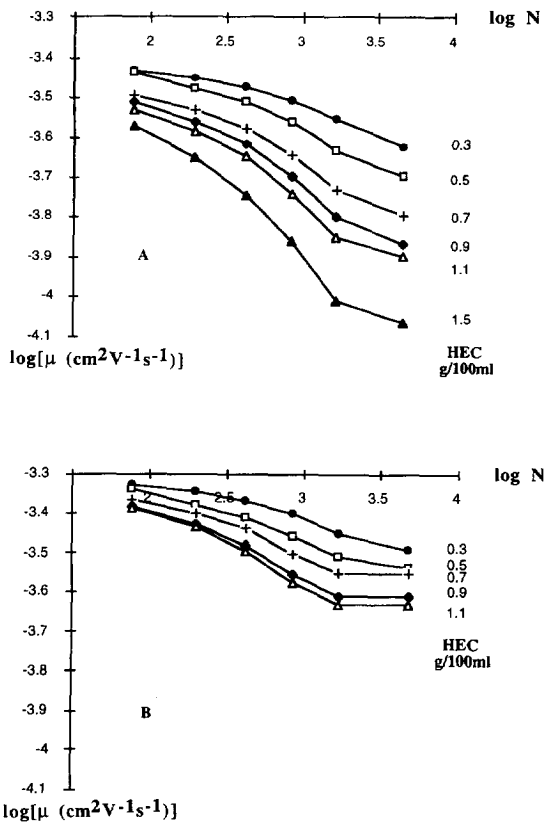

Fig. 12. Effect of electric field and HEC concentration on log μ versus log N graphs. Capillary: bare silica, 45 cm (detection, 25 cm)×50 μm I.D. Electrolyte: mentioned HEC solution in 40 m*M* sodium borate buffer, pH 9.2. Applied voltage: (A) 10 kV (E=220 V/cm); (B) 30 kV (E=670 V/cm). Other conditions as in Fig. 4.

Luckey for the case of single-stranded DNAs in polyacrylamide gel under a field strength of 200 V/cm [14]. It appears that the relative elongation undergone by M_r 88, 177, 350 and 990×10^3 PSSs (ca. 430, 860, 1700 and 4800 molecular size, respectively) was very similar to that of 200, 340, 450 and 660 base DNA, respectively. This comparison suggests that for a given molecular size, a PSS strand stretches less and is more rigid than a single-stranded DNA. In addition, $\Delta R/R$ was found to be proportional to $N^{1.2}$ for PSSs in this work, and to $N^{1.5}$ for single stranded DNAs in [14].

4.5.3. Reptation and biased reptation

Fig. 12 shows the graphs of the logarithm of the electrophoretic mobility, μ, against the molecular size N for various HEC concentrations and two

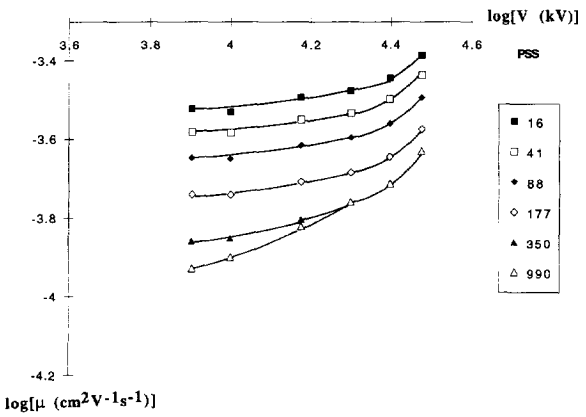

Fig. 13. Electric field dependence of the electrophoretic mobility for various PSS molecular mass. Capillary: bare silica, 45 cm (detection, 25 cm)×50 μm I.D. Electrolyte: 40 m*M* sodium borate buffer, pH 9.2, 1.1 g/100 ml HEC. Other conditions as in Fig. 4. PSS as in Fig. 7.

different electric field values. Typical sigmoidal curves are observed, as expected. In the case of a pure reptation regime, however, the graph should present a slope of -1 in the region of the inflexion point. Within the set of conditions studied, the maximal value calculated for the slope between two consecutive experimental points does not exceed 0.5. This result suggests that a direct transition between the Ogston regime and the biased reptation occurred and that pure reptation is not observed, probably because of the too high field strengths employed. It is seen that decreasing the field strength or increasing

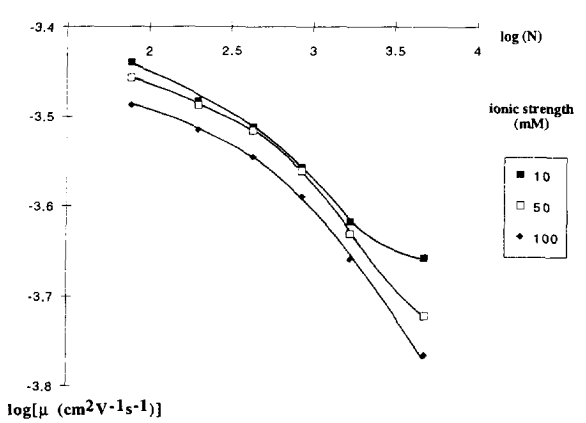

Fig. 14. Effect of ionic strength on log μ versus log N graphs. Capillary: bare silica, 45 cm (detection, 25 cm)×50 μm I.D. Electrolyte: sodium borate buffer of mentioned ionic strength, pH 9.2, 0.5 g/100 ml HEC. Other conditions as in Fig. 4.

the HEC concentration tended to render electrophoretic migration closer to a pure reptation regime for the PSSs of intermediate sizes. Furthermore, the typical mobility plateau corresponding to the ultimate behaviour of high-molecular-mass analytes in biased reptation is the more easily reached than field strength is greater and pore size narrower. Fig. 13 shows another graphical representation allowing us to illustrate the electric field dependence of mobility, for a given HEC concentration. Even in the zone of field strengths lower than 445 V/cm ($\log V < 4.3$), where Joule heating can be safely neglected, it is shown that the greater the PSS molecular mass is, the steeper the increase in mobility as field strength increases.

Fig. 14 shows the graph of $\log \mu$ against $\log N$ for various ionic strengths. It is interesting to note that an increase in the ionic strength renders the biased reptation plateau less visible, which can be explained by the decrease in the radius of gyration and the resulting decrease in solute sensitivity to deformation and orientation.

5. Concluding remarks

PSS separation according to molecular mass has proven feasible on a wide range (M_r $10–100\times10^3$), using capillary electrophoresis in entangled polymer solutions. The characteristic parameters, derived from viscosity measurements, were easily and successfully performed using a CE instrument, for both analyte and sieving polymers. The knowledge of these data has shed more light on migration mechanisms and helped to optimize conditions. A more exhaustive evaluation of sieving polymers with respect to their chemical nature and molecular mass is underway. This approach should also be of interest for molecular mass separation of various classes of synthetic and industrial ionic polymers.

Acknowledgments

We wish to thank J.L. Viovy, C. Heller and G.W. Slater for very helpful discussions.

References

[1] T.K. Wang, I. Illiopoulos and R. Audebert, Water Soluble Polymers, Synthesis and Solution Properties and Applications (ACS Symposium Series), American Chemical Society, Washington, DC, 1991, pp. 219–231.
[2] P.G. Righetti (Editor), Capillary Electrophoresis in Analytical Biotechnology, CRC Press, Boca Raton, FL, 1996.
[3] L.N. Amankwa, J. Scholl and W.G. Kuhr, Anal. Chem., 62 (1990) 2189–93.
[4] J. Bullock, J. Chromatogr., 645 (1993) 169–177.
[5] J.B. Poli and M.R. Schure, Anal. Chem., 64 (1992) 896–904.
[6] J. Sudor and M.V. Novotny, Anal. Chem., 1994 (66) 2139–2147.
[7] V. Dolnik and M.V. Novotny, Anal. Chem., 65 (1993) 563–67.
[8] S.V. Ermakov, M.Y. Zhukov, L. Capelli and P.G. Righetti, J. Chromatogr. A, 699 (1995) 297–313.
[9] M. Stefansson and M. Novotny, Anal. Chem., 66 (1994) 3466–3471.
[10] M.A.K. Williams, R.D. Keenan and D.M. Goodall, presented at the 7th Intern. Symp. on High Performance Capillary Electrophoresis, Würzburg, 1995, poster.
[11] P.D. Grossman and J.C. Colburn, Capillary Electrophoresis: Theory and Practice, Academic Press, San Diego, CA, 1992.
[12] A.G. Ogston, Trans. Faraday. Soc., 54 (1958) 237–256.
[13] D. Tietz and A. Chrambach, Electrophoresis, 14 (1993) 185–190.
[14] J.A. Luckey and L.M. Smith, Electrophoresis, 14 (1993) 492–501.
[15] V. Dolnik, J. Microcol. Sep., 6 (1994) 315–330.
[16] J.L. Viovy and T. Duke, Electrophoresis, 14 (1993) 322–329.
[17] L. Mitnik, L. Salomé, J.L. Viovy and C. Heller, J. Chromatogr. A, 710 (1995) 309–321.
[18] P.D. Grossman and D.S. Soane, Biopolymers, 31 (1991) 1221–1228.
[19] J.L. Viovy and C. Heller, in P.G. Righetti (Editor), Capillary Electrophoresis in Analytical Biotechnology, CRC Press, Boca Raton, FL, 1996, pp. 477–504.
[20] G.W. Slater and H.L. Guo, Electrophoresis, 16 (1995) 11–15.
[21] M. Chiari and M. Nesi, J. Chromatogr. A, 652 (1993) 31–39.
[22] M.S. Bello, R. Rezzonico and P.G. Righetti, J. Chromatogr. A, 659 (1994) 199–204.
[23] E.A. Bekturov, Z.K. Bakauova, Synthetic Water-Soluble Polymers in Solution, Hüthig and Wepf Verlag, Basel, 1986, p. 136.
[24] A.E. Barron, D. Soane and H.W. Blanch, J. Chromatogr. A, 659 (1993) 3–16.
[25] A.E. Barron, D. Soane and H.W. Blanch, Electrophoresis, 15 (1994) 597–615.